ORIGINAL RESEARCH

Extracellular Vesicles from Fibroblasts Induce Epithelial-Cell Senescence in Pulmonary Fibrosis

Tsukasa Kadota[1,2], Yusuke Yoshioka[1,3], Yu Fujita[1,2], Jun Araya[2], Shunsuke Minagawa[2], Hiromichi Hara[2], Atsushi Miyamoto[4], Souichiro Suzuki[5], Sakashi Fujimori[5], Tadasu Kohno[5], Takeshi Fujii[6], Kazuma Kishi[4], Kazuyoshi Kuwano[2], and Takahiro Ochiya[1,3]

[1]Division of Molecular and Cellular Medicine, National Cancer Center Research Institute, Tokyo, Japan; [2]Division of Respiratory Diseases, Department of Internal Medicine, The Jikei University School of Medicine, Tokyo, Japan; [3]Department of Molecular and Cellular Medicine, Institute of Medical Science, Tokyo Medical University, Tokyo, Japan; and [4]Department of Respiratory Medicine, Respiratory Center, [5]Department of Thoracic Surgery, and [6]Department of Pathology, Toranomon Hospital, Tokyo, Japan

ORCID IDs: 0000-0002-9533-7241 (T. Kadota); 0000-0002-8916-7303 (Y.F.); 0000-0003-1732-4856 (S.M.); 0000-0002-3444-0536 (A.M.).

Abstract

Aberrant epithelial–mesenchymal interactions have critical roles in regulating fibrosis development. The involvement of extracellular vesicles (EVs), including exosomes, remains to be elucidated in the pathogenesis of idiopathic pulmonary fibrosis (IPF). Here, we found that lung fibroblasts (LFs) from patients with IPF induce cellular senescence via EV-mediated transfer of pathogenic cargo to lung epithelial cells. Mechanistically, IPF LF–derived EVs increased mitochondrial reactive oxygen species and associated mitochondrial damage in lung epithelial cells, leading to activation of the DNA damage response and subsequent epithelial-cell senescence. We showed that IPF LF-derived EVs contain elevated levels of microRNA-23b-3p (miR-23b-3p) and miR-494-3p, which suppress *SIRT3*, resulting in the epithelial EV-induced phenotypic changes. Furthermore, the levels of miR-23b-3p and miR-494-3p found in IPF LF–derived EVs correlated positively with IPF disease severity. These findings reveal that the accelerated epithelial-cell mitochondrial damage and senescence observed during IPF pathogenesis are caused by a novel paracrine effect of IPF fibroblasts via microRNA-containing EVs.

Keywords: exosome; fibroblast; epithelial cell; cellular senescence; mitochondrial damage

Clinical Relevance

Lung epithelial cell senescence is crucial for the initiation and progression of fibrosis in idiopathic pulmonary fibrosis. Currently, the exact mechanisms remain unknown. This study reveals that lung fibroblast–derived extracellular vesicles induce epithelial-cell mitochondrial damage and senescence during the development of fibrosis. Our findings suggest that lung fibroblast–derived extracellular vesicles act as a novel paracrine mediator in the pathogenesis of idiopathic pulmonary fibrosis.

Idiopathic pulmonary fibrosis (IPF) is a chronic, progressive, irreversible, and fatal interstitial lung disease with a median survival of only 3–5 years from the time of diagnosis (1). It is noteworthy that the incidence and prevalence of IPF increase significantly with age (1). Indeed, increased epithelial-cell senescence, which is a prominent feature of aging, is a part of the stress response that characterizes IPF. Damaged cells experience irreversible growth arrest and develop a complex senescence-associated secretory

(Received in original form January 2, 2020; accepted in final form July 6, 2020)

Supported in part by a Grant-in-Aid for the Japan Science and Technology Agency through the Center of Open Innovation Network for Smart Health initiated by the Council for Science; the Basic Science and Platform Technology Program for Innovative Biological Medicine from Japan Agency for Medical Research and Development (AMED); the Practical Research Project for Rare Intractable Diseases from AMED; the Ministry of Health, Labor and Welfare of Japan awarded to the Study Group on Diffuse Pulmonary Disorders, Scientific Research/Research on intractable diseases; and GSK Japan Research Grant 2016.

Author Contributions: T. Kadota, Y.F., and J.A. conceived and designed the study. T. Kadota and Y.F. performed the experiments and data analysis. T. Kadota, Y.Y., Y.F., J.A., S.M., H.H., and K. Kuwano interpreted the data. T. Kadota wrote the manuscript. Y.Y., Y.F., J.A., and K. Kuwano assisted with the manuscript and provided helpful discussion. A.M., S.S., S.F., T. Kohno, T.F., and K. Kishi provided the patients' samples. T.O. supervised this project.

Correspondence and requests for reprints should be addressed to Takahiro Ochiya, Ph.D., National Cancer Center Research Institute, 5-1-1 Tsukiji, Chuo-ku, Tokyo 104-0045, Japan. E-mail: tochiya@ncc.go.jp.

This article has a related editorial.

This article has a data supplement, which is accessible from this issue's table of contents at www.atsjournals.org.

Am J Respir Cell Mol Biol Vol 63, Iss 5, pp 623–636, Nov 2020

Originally Published in Press as DOI: 10.1165/rcmb.2020-0002OC on July 30, 2020
Internet address: www.atsjournals.org

phenotype (SASP) (2). Recent advances indicate a mechanistic link between IPF pathogenesis and the accumulation of senescent epithelial cells (3–6). However, the exact mechanisms responsible for accelerated cellular senescence in IPF remain unknown.

Lung epithelial cells adjacent to myofibroblasts in fibroblastic foci are the leading edge of fibrotic development (7), and they exhibit cellular senescence, together with abnormal morphology and gene-expression patterns (3, 8, 9). Accumulating evidence shows that senescent epithelial cells produce a variety of growth factors, cytokines, and proteinases that provoke the migration, proliferation, and activation of fibroblasts. This represents one underlying mechanism for the aberrant epithelial–mesenchymal interactions that characterize IPF pathogenesis (3, 7, 10). Lung fibroblasts (LFs) derived from IPF tissue also exhibit distinct alterations in gene-expression profiles (11–13) and are known to produce factors that affect not only the fibroblast phenotype but also epithelial-cell proliferation and apoptosis (14–16). However, the importance of aberrant fibroblast–epithelial cross-talk in regulating IPF-related lung epithelial-cell senescence remains largely unknown.

Extracellular vesicles (EVs), including exosomes and microvesicles, are increasingly recognized as regulatory mediators of intercellular communication via the transfer of their bioactive molecular cargos such as microRNAs (miRNAs) (17, 18). MiRNAs are small endogenous noncoding RNAs that regulate genes at the transcriptional and posttranscriptional levels by binding to the 3′-untranslated regions (UTRs) of target mRNAs. In the lung, EV-associated miRNAs participate in normal tissue homeostasis as well as in a variety of lung pathologies (19). Notably, EVs derived from fibroblasts have been shown to play pathogenic roles in the microenvironment (20, 21). Thus, it is conceivable that in IPF pathogenesis, EV-associated miRNAs derived from fibroblasts might mediate aberrant fibroblast–epithelial cell cross-talk that leads to epithelial-cell senescence. Here, we use clinical samples to investigate whether IPF LF–derived EVs transfer key miRNA species to lung epithelial cells to contribute to IPF-related phenotypic alterations in epithelial cells, including accelerated cellular senescence.

Methods

For a detailed description of the Methods used in this work, *see* the data supplement.

Cell Culture and Clinical Samples

All human lung tissues were obtained from pneumonectomy or lobectomy specimens at The Jikei University Hospital and Toranomon Hospital. LFs and human bronchial epithelial cells (HBECs) were isolated and characterized from explant cultures in the same way as previously described (22). Briefly, fibroblasts outgrown from lung fragments were cultured in Dulbecco's modified Eagle's medium (11965-092; Gibco Life Technologies) with a 10% FBS (26140-079; Gibco Life Technologies) and a 1% antibiotic–antimycotic solution (AA; Invitrogen) at 37°C in 5% CO_2. LFs were serially passaged when the cells had reached ∼80–100% confluence and were actively proliferating, and these cells were used for experiments until passage 6. HBECs were isolated using protease treatment from normal airways from first- through fourth-order bronchi or were purchased from Lonza. Freshly isolated HBECs were plated onto Rat Tail and collagen type I–coated dishes in bronchial epithelial growth medium (Lonza). HBECs were used until passage 4.

Table 1. Patient Characteristics (for Lung Fibroblasts)

	Non-IPF ($n = 26$)	IPF ($n = 20$)	*P* Value
Age, yr	67.5 ± 8.2	71.4 ± 6.0	NS
Males, % of group	61.5	80.0	NS
SI, pack-years	16.7 ± 33.1	66.8 ± 65.8	0.0016
%VC	108.3 ± 14.2	90.63 ± 15.8	<0.001
FEV_1/FVC (%)	77.8 ± 10.74	74.3 ± 10.41	NS

Definition of abbreviations: FEV_1 = forced expiratory volume in 1 second; FVC = forced vital capacity; IPF = idiopathic pulmonary disease; NS = no significance; SI = smoking index; VC = vital capacity. Values are mean ± SD.

Human small-airway epithelial cells were isolated from the distal portion of the lung tissue. A piece of lung tissue was mechanically minced and dissociated with enzymes according to the Lung Dissociation Kit protocol (130-095-927; Miltenyi Biotec). A Miltenyi Biotec gentle MACS dissociator was used for mincing and incubation for 42 minutes at 37°C. Cells were washed and passed over 70-μM and 40-μM filters, and red blood cells were lysed with red-blood-cell lysis buffer (42574000; Miltenyi Biotec). After a cell suspension was obtained, cells were cultured in small-airway epithelial-cell growth medium (basal medium plus growth supplements, CC-3118; Lonza) and a 1% AA at 37°C in 5% CO_2. Human embryonic kidney 293 (HEK293) cell was cultured in Dulbecco's modified Eagle's medium with 10% FBS supplemented with a 1% AA at 37°C in 5% CO_2. Non-IPF participants had no history of pulmonary fibrosis, chronic obstructive pulmonary disease, or any other inflammatory diseases. The diagnosis of IPF was based on an international consensus statement by the American Thoracic Society and the European Respiratory Society. All patients had a usual interstitial pneumonia pattern on high-resolution computed tomographic images of the chest. Patients with alternative explanations for interstitial lung disease, such as connective-tissue disease–associated, hypersensitivity pneumonitis, radiation treatment, drug-induced disease, occupation-associated disease, and sarcoidosis were excluded. The relevant characteristics of patients are summarized in Table 1 and Table E1 (*see* the data supplement).

Results

Characterization of LF-derived EVs from Patients with IPF

To investigate the role of LF-derived EVs in IPF pathogenesis, primary LF cultures were established from lung tissues taken from 20 patients with IPF and 26 individuals without IPF (Table 1). To characterize the IPF LFs, we evaluated the expression levels of ACTA2, which is a representative marker for myofibroblast differentiation. Immunohistochemical examination of intact lung tissue shows that α-SMA–positive LFs are much more abundant in fibrotic lesions in IPF lungs than in healthy lungs (*see* Figure E1A in the data supplement). Western blotting and quantitative real-time

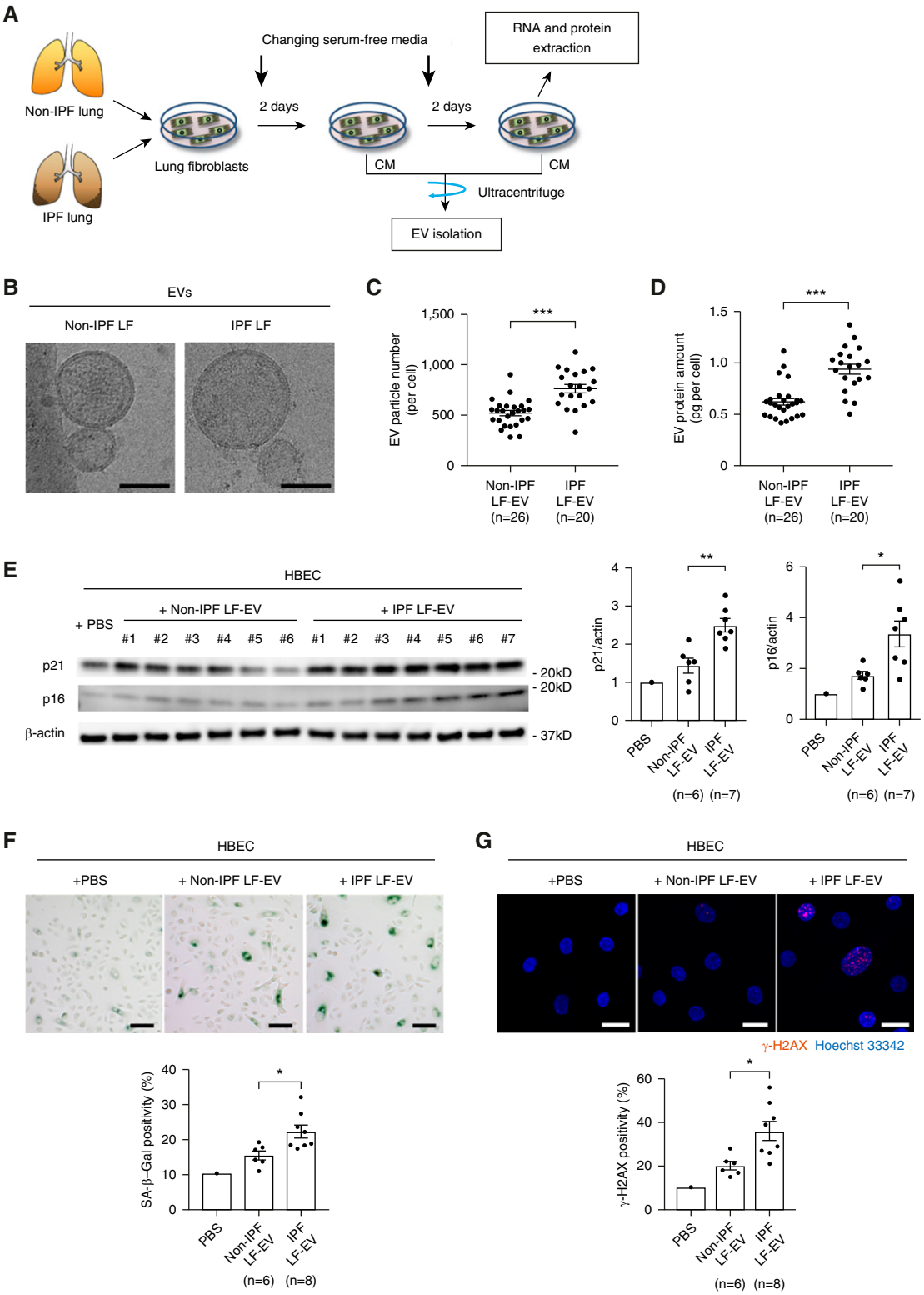

Figure 1. Extracellular vesicles (EVs) from idiopathic pulmonary fibrosis (IPF) lung fibroblasts (LFs) accelerate cellular senescence and mitochondrial damage in human bronchial epithelial cells (HBECs). (*A*) Schematic protocol for the isolation of EVs and extraction of RNA and protein from IPF LFs and non-IPF LFs. (*B*) EM of isolated EVs from IPF LFs and non-IPF LFs. Scale bars, 100 nm. (*C*) Comparison of the particle numbers of IPF LF–derived EVs and non-IPF LF–derived EVs. The vertical axis in the graphs shows the number of EV particles/cells. Error bars represent the SEM. ***$P < 0.0005$. (*D*) Comparison of the protein amounts in IPF LF–derived EVs and non–IPF LF–derived EVs. The vertical axis in the graphs shows the amount of EV protein

PCR analyses of cultured LFs further confirm that α-SMA expression levels are increased in cultures of IPF LFs compared with cultures of non-IPF LFs (Figures E1B and E1C). Moreover, in IPF LFs, high expression of p21 (CDKN1A) and p16 (CDKN2A) (senescence-associated cyclin-dependent kinase inhibitors) was revealed using Western blotting (Figure E1D), and high expressions of p21 and SASP mRNAs such as IL-6 and IL-1β were revealed using quantitative real-time PCR (Figure E1E). These results indicate that IPF LFs have several distinct phenotypes, such as myofibroblast and/or senescent LFs.

To characterize the production of EVs by LFs, we used ultracentrifugation to isolate EVs from serum-free culture media of both IPF and non-IPF LFs (Figure 1A). Cryotransmission EM revealed bilayer membrane structures with a size range of 50–150 nm in both sets of EV isolates (Figures 1B and E1F). The size distribution of LF-derived EVs, as measured by nanoparticle-tracking analysis, confirms a size range between 50 and 150 nm with no significant difference between IPF LFs and non-IPF LFs (Figure E1G). Western blotting analysis revealed the presence of the EV marker proteins CD9, CD63, CD81, Hsc70, and Caveolin-1 in both sets of LF-derived EVs, whereas the mitochondrial protein Tomm20 and the actin cytoskeleton were not enriched in the EVs (Figure E1H). These data suggest that the EV populations isolated from LF-conditioned media are mainly composed of exosomes. In addition, we found that the EV particle numbers of EVs derived from IPF LFs were significantly increased compared with the numbers of those derived from non-IPF LFs (Figures 1C and D and E1I).

IPF LF–derived EVs Evoke a DNA Damage Response and Induce Senescence in Human Lung Epithelial Cells

Fibroblast-derived EVs are known to exert a variety of pathological effects within their microenvironments (20, 21, 23), suggesting a paracrine role for IPF LF–derived EVs in modulating an epithelial-cell phenotype. We previously observed accelerated cellular senescence in metaplastic epithelial cells originating from bronchioles of IPF lungs (3, 24), so we selected primary HBECs as targets for assessing the effects of IPF LF–derived EVs on cellular senescence. Initially, we examined HBEC uptake of LF-derived EVs labeled with the fluorescent dye PKH67 (Figures E1J and E1K). Confocal microscopy revealed the uptake of labeled LF-derived EVs by HBECs. To elucidate the effect of IPF LF–derived EVs on the epithelial-cell phenotype, we compared the effects of incubating HBECs with LF-derived EVs from patients with IPF or from individuals without IPF. Interestingly, treatment of HBECs with IPF LF–derived EVs clearly induces concentration-dependent epithelial-cell senescence, as shown by p21 and p16 expression levels, which were higher than those observed in cells treated with control EVs (Figures 1E and E1L). In addition, increased staining for SA-β-gal (senescence-associated-β–galactosidase) was observed in HBECs treated with IPF LF–derived EVs (Figure 1F). The DNA damage response (DDR) is a crucial initiator of cellular senescence that is initiated via activation of the p53/p21 and/or p16/pRb pathways (25). Induction of the DDR in IPF LF–derived EV-treated HBECs is demonstrated by the increased number of γ-H2AX (phospho-Histone H2A.X)–positive nuclei (Figures 1G and E1M). Furthermore, we validated that IPF LF–derived EVs induce cellular senescence in primary human small-airway epithelial cells, which are isolated from peripheral airways in normal human lung tissue, as shown by p21 and p16 expression levels and staining for SA-β-gal (Figures E1N and E1O). Taken together, these results suggest that IPF LF–derived EVs increase lung epithelial-cell senescence by activating the DDR.

IPF LF–derived EVs Induce Mitochondrial Reactive-Oxygen-Species Production and Mitochondrial Damage in Lung Epithelial Cells

To further elucidate the IPF LF–derived EV-dependent mechanisms that underlie accelerated senescence in HBECs, we evaluated reactive-oxygen-species (ROS) production in these cells. It is widely recognized that increases in ROS, which are mainly produced by mitochondria, are involved in the induction of a persistent DDR with concomitant cellular senescence (25–28). Accordingly, we measured intracellular ROS and mitochondrial ROS (mtROS) production in HBECs in response to EV treatment. HBECs incubated with IPF LF–derived EVs exhibited increases in both intracellular ROS production, as measured by the 2′,7′-dichlorofluorescin diacetate (DCFH-DA) assay (Figure 2A), and mtROS production, as measured by MitoSOX Red staining (Figure 2B). Notably, both *N*-acetylcysteine (an efficient antioxidant that reduces intracellular ROS) and Mito-TEMPO (a specific antioxidant that reduces mtROS) efficiently inhibited the increase in mtROS production induced by IPF LF–derived EVs (Figure E2A), DDR activation (Figure 2C), and HBEC senescence (Figure 2D). These results suggest the involvement of mtROS in the mechanisms responsible for aberrant activation of the DDR and induction of HBEC senescence by IPF LF–derived EVs.

Because type II alveolar epithelial cells in IPF lungs exhibit structural and functional alterations in their mitochondria (29), we reasoned that there might be a link between elevated mtROS production and mitochondrial damage in the epithelial-cell response to IPF LF-derived EV treatment. In tests of mitochondrial function, we found that treatment of HBECs with IPF LF-derived EVs significantly decreased intracellular levels of ATP, the key product of mitochondria, relative to the levels seen in cells treated with non-IPF LF-derived EVs (Figure 2E). To identify possible alterations

Figure 1. (*Continued*). ($\times 10^6$)/cell. Error bars represent the SEM. ***$P < 0.0005$. (*E*) Western blot using anti-p21, anti-p16, and anti–β-actin antibodies of cell lysates from HBECs incubated with non-IPF LF–derived EVs (10 μg/ml, $n = 6$), IPF LF–derived EVs (10 μg/ml, $n = 7$), or non-EV controls for 72 hours. The right panel shows the average (±SEM) of relative expressions, which are taken from densitometric analysis of Western blotting. *$P < 0.05$ and **$P < 0.005$. (*F*) Representative images of SA-β-gal (senescence-associated-β–galactosidase) staining in HBECs incubated with non-IPF LF–derived EVs (10 μg/ml, $n = 6$), IPF LF–derived EVs (10 μg/ml, $n = 8$), or non-EV controls for 72 hours. The right panel shows the percentage (±SEM) of SA-β-gal–positive cells. *$P < 0.05$. Scale bars, 50 μm. (*G*) Representative images of γ-H2AX (phospho-Histone H2A.X) and Hoechst 33342 staining in HBECs incubated with non-IPF LF–derived EVs (10 μg/ml, $n = 6$), IPF LF–derived EVs (10 μg/ml, $n = 8$), or non-EV controls for 48 hours. The right panel shows the percentage of γ-H2AX–positive cells. *$P < 0.05$. Scale bars, 20 μm. CM = conditioned medium.

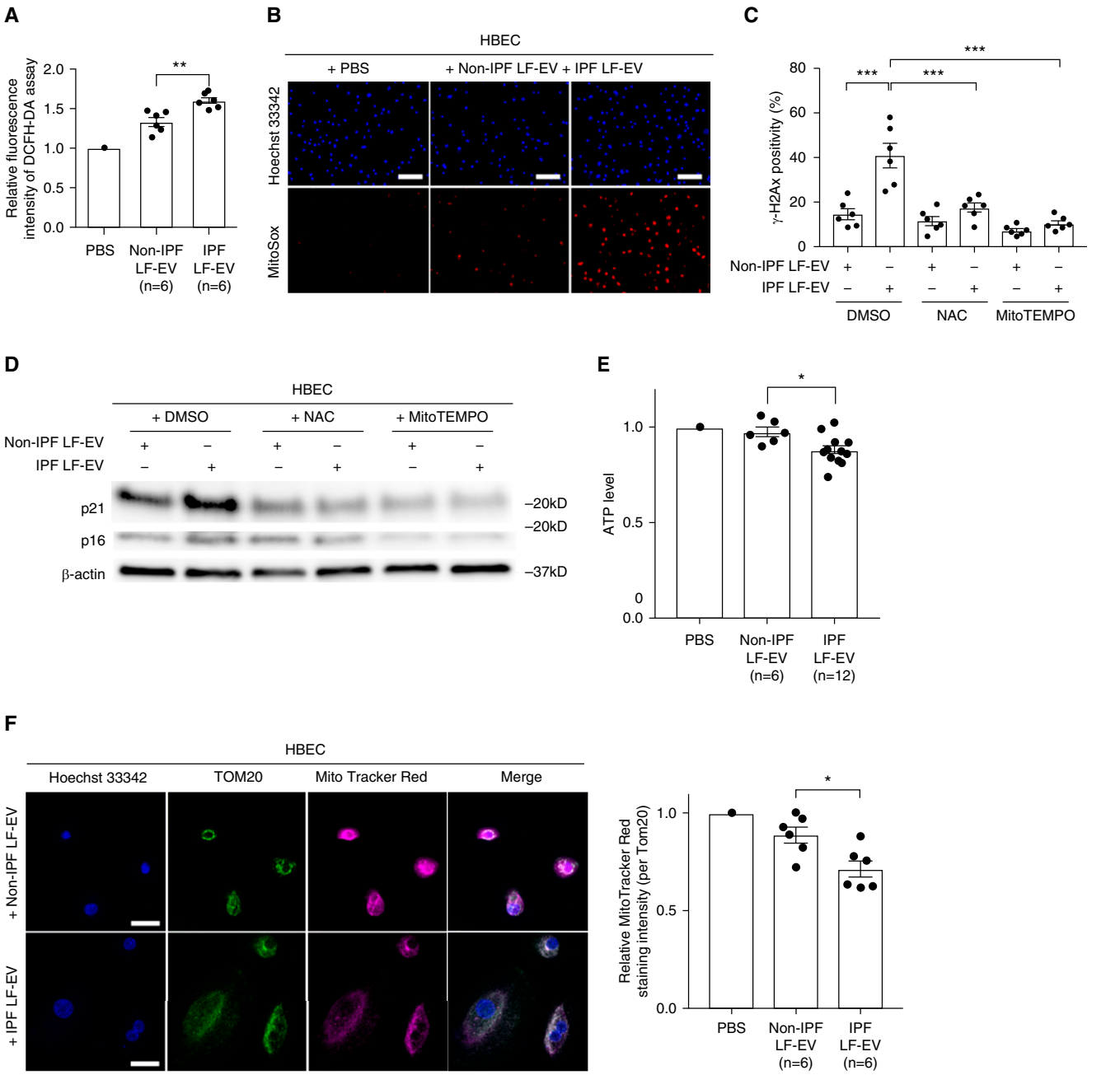

Figure 2. IPF LF–derived EVs regulate mitochondrial reactive oxygen species (mtROS) production and mitochondrial damage in HBECs. (*A*) Fluorescence intensity of 2′,7′-dichlorodihydrofluorescein diacetate (DCFH-DA) staining for intracellular ROS production. Incubation with DCFH-DA was started at 48 hours after incubation of non-IPF LF–derived EVs (10 μg/ml, $n = 6$), IPF LF–derived EVs (10 μg/ml, $n = 6$), or non-EV controls in HBECs. $^{**}P < 0.005$. (*B*) Representative images of Hoechst 33342 and MitoSOX Red fluorescence staining in HBECs incubated with non-IPF LF–derived EVs (10 μg/ml), IPF LF–derived EVs (10 μg/ml), or non-EV controls for 48 hours. Scale bars, 100 μm. (*C*) The percentage of γ-H2AX–positive cells in control-treated, *N*-acetylcysteine (NAC; 2 mM)–treated, and Mito-TEMPO (100 μM)–treated HBECs for 48 hours. Pretreatment was conducted with NAC and Mito-TEMPO for 1 hour before treatment of non-IPF LF–derived EVs (10 μg/ml, $n = 6$) or IPF LF–derived EVs (10 μg/ml, $n = 6$). $^{***}P < 0.0005$, Sidak multiple-comparison testing after one-way ANOVA. (*D*) Western blot using anti-p21, anti-p16, and anti–β-actin in control-treated, NAC (2 mM)–treated, and Mito-TEMPO (100 μM)–treated HBECs for 72 hours. Pretreatment was conducted with NAC and Mito-TEMPO for 1 hour before non–IPF LF–derived EVs (10 μg/ml) or IPF LF–derived EVs (10 μg/ml). (*E*) Intracellular ATP levels were determined after incubation with non-IPF LF–derived EVs (10 μg/ml, $n = 6$), IPF LF–derived EVs (10 μg/ml, $n = 12$), or non-EV controls for 72 hours in HBECs. Data shown represent the mean ± SEM in each group. $^{*}P < 0.05$. (*F*) Representative fluorescence microscopy images showing the cellular distribution of the mitochondria-specific dye MitoTracker Red (magenta) and TOM20 (the mitochondrial import receptor subunit homolog; green). Relative MitoTracker Red staining intensity within mitochondria was quantified using TOM20 to generate a mask of the mitochondrial area. HBECs were incubated with IPF LF–derived EVs (10 μg/ml), non-IPF LF–derived EVs (10 μg/ml), or non-EV controls for 72 hours. Scale bars, 20 μm. Data shown represent the mean ± SEM in each group. $^{*}P < 0.05$.

in the functional integrity of mitochondria, we performed immunofluorescence staining of EV-treated HBECs with anti-TOM 20 (to visualize the mitochondrial outer membrane) and with MitoTracker Red (to evaluate mitochondrial membrane potential) (Figure 2F). IPF LF–derived EV treatment decreased MitoTracker Red staining intensity within the mitochondrial area, indicating that IPF LF–derived EVs can induce accumulation of dysfunctional mitochondria in HBECs.

Differential miRNA Profiles in Non-IPF and IPF LF–derived EVs

To explore in more detail the molecular mechanisms by which IPF LF–derived EVs induce HBEC senescence via the mtROS-mediated DDR pathway, we compared the biomolecular cargo present in IPF LF–derived EVs and non-IPF LF–derived EVs. EVs are known to encapsulate significant quantities of miRNAs that can be transferred to and can function in EV-targeted cells (17, 18). Importantly, we found that LF-derived EVs contain an abundance of small RNAs, including miRNAs (Figure E4). Accordingly, the expression profiles of miRNAs in non-IPF and IPF LF–derived EVs were examined by miRNA microarray analysis. For this purpose, we pooled six of the individual IPF LF–derived EV samples and six of the individual non-IPF LF–derived EV samples (Figure 3A). Among the differentially expressed miRNAs, 27 upregulated miRNAs from IPF LF–derived EVs were selected for further validation (Figure 3B). Quantitative real-time PCR evaluation of the 27 miRNA candidates in all 46 individual EV samples (IPF, $n = 20$; non-IPF, $n = 26$;) (Table 1) revealed that six miRNAs (miR-19a-3p, miR-23b-3p, miR-127-3p, miR-145-5p, miR-424-5p, and miR-494-3p) were significantly upregulated in IPF LF–derived EVs compared with non-IPF LF–derived EVs (Figure 3C). There was no significant difference in the expression levels of cellular miR-19a-3p, miR-127-3p, miR-424-5p and miR-494-3p between IPF LFs and non-IPF LFs, implying that these

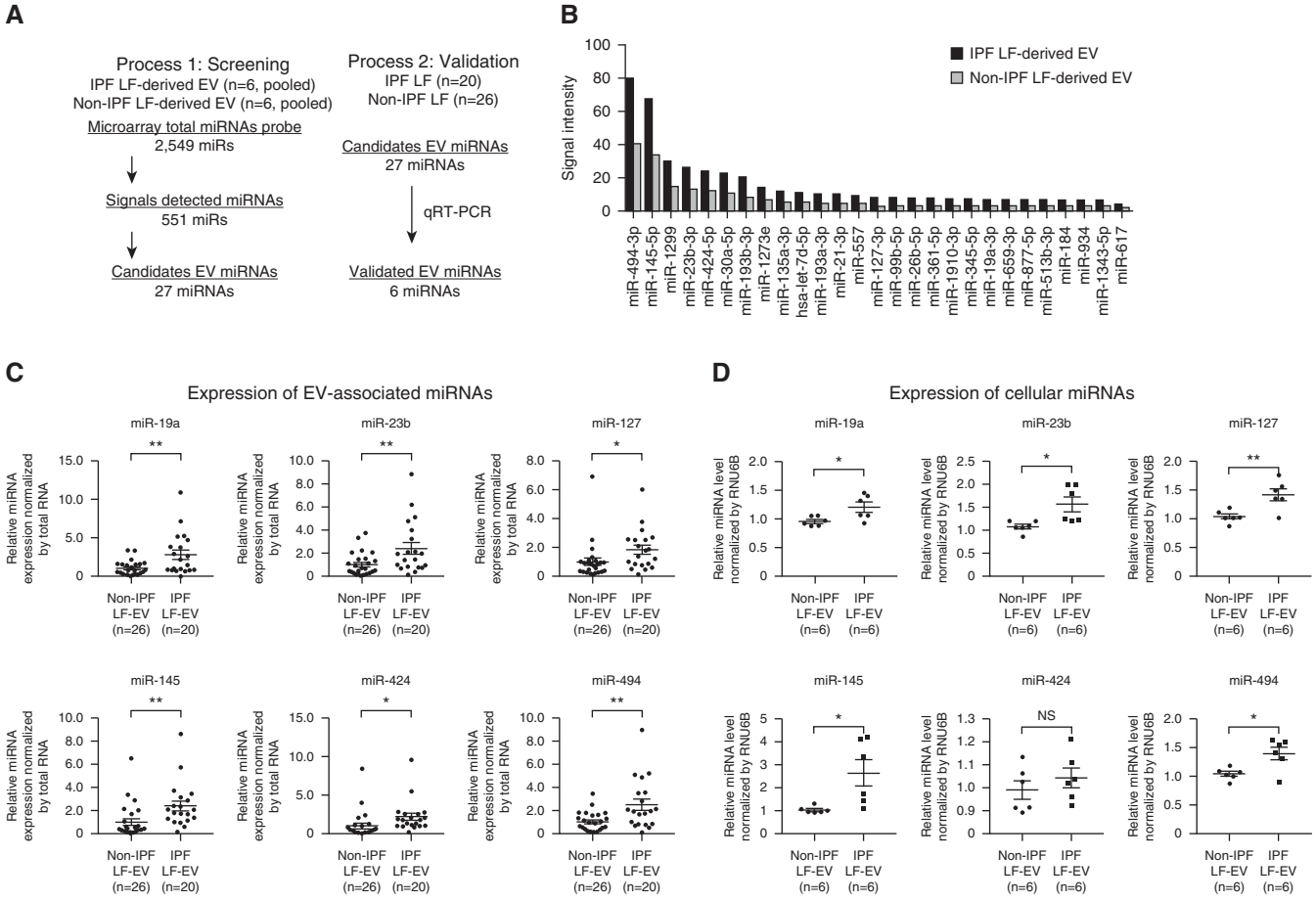

Figure 3. MicroRNA (miRNA) profile in IPF LF–derived EVs and non-IPF LF–derived EVs. (*A*) An overview of the process for identification of upregulated miRNAs in IPF LF–derived EVs compared with non-IPF LF–derived EVs. In the screening process, miRNAs in LF-derived EVs were analyzed from two samples that were pooled from six individual IPF LF–derived EVs and six individual non-IPF LF–derived EV samples by miRNA microarray. Candidates' miRNAs that were upregulated in IPF LF–derived EVs compared with non-IPF LF were selected on the basis of two filtering criteria (fold change > 1.4; the named number of miRNAs < 2,000). Among the EV-associated miRNAs, 27 were selected for further consideration by quantitative real-time PCR validation. In the next process, six EV-associated miRNAs were validated using LF-derived EVs from patients with IPF ($n = 26$) and individuals without IPF ($n = 20$). (*B*) Microarray signal intensity of the 27 candidate miRNAs in IPF LF–derived and non-IPF LF–derived EVs. (*C*) Quantitative real-time PCR validation of miRNAs in IPF LF–derived EVs ($n = 20$) and non-IPF LF–derived EVs ($n = 26$). Total RNA was used as an internal control. $^{*}P < 0.05$ and $^{**}P < 0.005$. (*D*) Quantitative real-time PCR analysis of cellular miRNA expressions in HBECs incubated with IPF LF–derived EVs (10 μg/ml, $n = 6$) or non-IPF LF–derived EVs (10 μg/ml, $n = 6$) for 24 hours. RNU6B was used as an internal control. $^{*}P < 0.05$ and $^{**}P < 0.005$. NS = no significance.

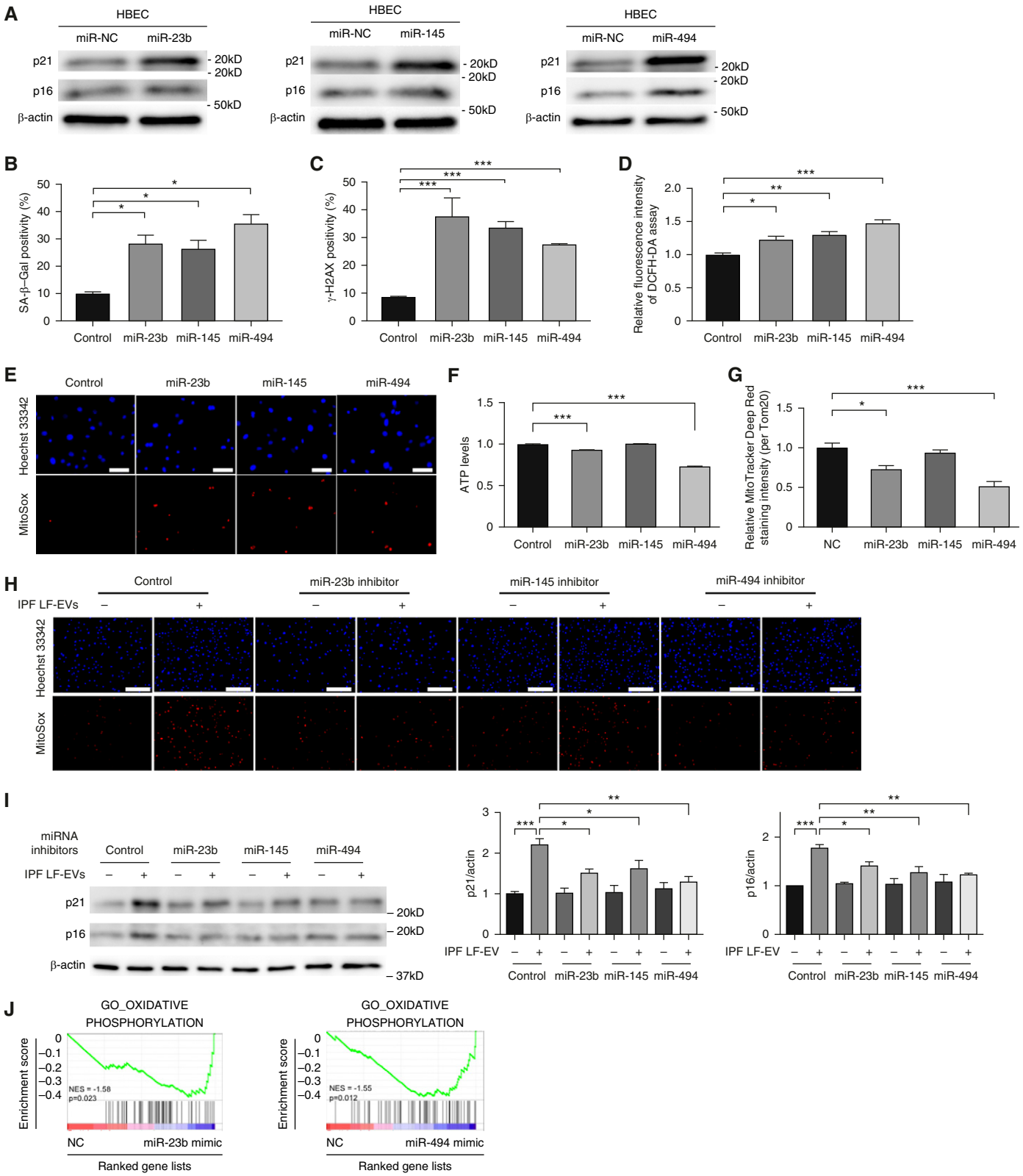

Figure 4. Transfer of miR-23b-3p and miR-494-3p via IPF LF–derived EVs induces mitochondrial damage and senescence in HBECs. (*A*) Western blot using anti-p21, anti-p16, and anti–β-actin antibodies in HBECs transfected with miR-23b-3p, miR-145-5p, miR-494-3p, or negative control (NC) for 72 hours. (*B*) The percentage (±SEM) of SA-β-gal–positive cells in HBECs transfected with miR-23b-3p mimic, miR-145-5p mimic, miR-494–3p mimic, or NC for 72 hours. *$P < 0.05$. (*C*) The percentage of γ-H2AX–positive cells in HBECs transfected with miR-23b-3p mimic, miR-145-5p mimic, miR-494-3p

miRNAs are selectively encapsulated in IPF LF–derived EVs (Figure E3B). To assess the EV-mediated transfer of these six miRNAs to HBECs, we evaluated miRNA expression levels in HBECs after treatment with IPF LF–derived EVs and non-IPF LFs. As shown in Figure 3D, HBEC expression levels of miR-19a-3p, miR-23b-3p, miR-127-3p, miR-145-5p, and miR-494-3p were significantly higher after treatment with IPF LF–derived EVs than those after treatment with non-IPF LF–derived EVs, indicating the efficient transfer of these five miRNAs into recipient HBECs (Figure 3D).

Transfer of miR-23b-3p and miR-494–3p via IPF LF–derived EVs Induces Mitochondrial Damage and Senescence in Lung Epithelial Cells

To determine whether specific miRNAs initiate mitochondrial damage, mtROS-mediated activation of DDR, and cellular senescence in lung epithelial cells, we examined the direct effects of the five validated miRNAs on HBEC biology. Transfection of the five synthesized miRNA mimics into HBECs revealed that miR-23b-3p, miR-145-5p and miR-494-3p induced p21 and p16 expression (Figures 4A and E4A), enhanced staining of SA-β-gal (Figures 4B and E4B), and increased the number of γ-H2AX-positive foci (Figures 4C and E4C). These transfection experiments also demonstrated the involvement of miR-23b-3p, miR-145-5p and miR-494-3p in mtROS production and mitochondrial damage. HBECs transfected with miR-23b-3p and miR-494-3p exhibited significantly increased production of intracellular ROS and mtROS production (Figures 4D and 4E), which was accompanied by decreased intracellular ATP levels and decreased mitochondrial-membrane potential (Figures 4F, 4G, and E4D). In contrast, HBECs transfected with miR-145-5p showed significantly enhanced intracellular ROS and mtROS production, but they showed no decreases in intracellular ATP levels or mitochondrial-membrane potential. The specificity of these effects is supported by our finding that increases in mtROS (Figure 4H), the DDR (Figure E4E), and cellular senescence (Figure 4I) induced by IPF LF–derived EVs in HBECs are attenuated by treating the cells with inhibitors of miR-23b-3p, miR-145-5p, and miR-494-3p. To further show the specificity of these effects by miR-23b-3p, miR-145-5p, or miR-494-3p in IPF LF–derived EVs, we collected these miRNA-enriched EVs, which were isolated from transiently overexpressing IPF LFs. After transfection of miR-23b-3p, miR-145-5p, or miR-494-3p mimics into IPF LFs, their expression was increased not only in the cells (Figure E4F) but also in the EVs (Figure E4G). The incubation of these miRNA-enriched EVs in HBECs increased the expression of p21 and p16 (Figure E4H). Moreover, the increases in p21 and p16 expression in HBECs by EVs derived from IPF LFs was attenuated when IPF LFs were transfected with miR-23b-3p, miR-145-5p, or miR-494-3p inhibitors (Figure E4I). Taken together, these data support the notion that these key miRNAs play a pivotal role in promoting HBEC senescence in response to treatment with IPF LF–derived EVs.

To elucidate possible mechanisms underlying the effects of miRNAs on mitochondrial damage and cellular senescence, mRNA microarray analysis was performed. Gene-set enrichment analyses revealed that genes associated with oxidative phosphorylation, the critical activity of mitochondria, are significantly downregulated in HBECs transfected with miR-23b-3p and miR-494-3p mimics (Figure 4J). A downward trend in these same genes was also seen in HBECs transfected with the miR-145-5p mimic (Figure E4F). These findings suggest that miR-23b-3p and miR-494-3p are primarily responsible for mitochondrial damage, enhanced mtROS production, and cellular senescence induced in HBECs by IPF LF–derived EVs.

Reduced Expression of SIRT3 Is Involved in miR-23b-3p– and miR-494-3p–Mediated Mitochondrial Damage and Cellular Senescence

To determine how miR-23b-3p and miR-494-3p mediate mitochondrial damage and cellular senescence in response to EV treatment, we sought to identify genes that are targeted by these miRNAs in HBECs. Because both of these miRNAs induce similar phenotypes in HBECs, it is plausible that both miRNAs may target the same gene products to alter mitochondrial function. *In silico* analysis using TargetScan Human 7.2 (www.targetscan.org) and Human MitoCarta 2.0 (30) allowed us to identify and select 10 putative target genes for miR-23-3p and miR-494-3p action (Figure 5A). Among the 10 predicted target genes, expression levels of *SIRT3* (Sirtuin 3), *BCKDHB* (Branched Chain Keto Acid Dehydrogenase E1 Subunit β), *SLC25A40* (Solute Carrier Family 25 Member 40), *SLC25A51* (Solute Carrier Family

Figure 4. (*Continued*). mimic, or NC from three independent experiments for 48 hours. ***$P < 0.0005$. (*D*) Fluorescence intensity of DCFH-DA staining for intracellular ROS production. Incubation with DCFH-DA was started at 48 hours after transfection of miR-23b-3p mimic, miR-145-5p mimic, miR-494-3p mimic, or NC in HBECs. Data shown represent the mean ± SEM of $n = 6$ in each group. *$P < 0.05$, **$P < 0.005$, and ***$P < 0.0005$, Sidak multiple-comparison testing after one-way ANOVA. (*E*) Representative images of Hoechst 33342 and MitoSOX Red fluorescence staining in HBECs transfected with miR-23b-3p, miR-145-5p, or miR-494-3p mimics for 48 hours from three independent experiments. Scale bars, 100 μm. (*F*) Intracellular ATP levels were determined after transfection of miR-23b-3p, miR-145-5p, or miR-494-3p mimics or NC for 72 hours in HBECs. Data shown represent the mean ± SEM of $n = 6$ in each group. ***$P < 0.0005$, unpaired *t* test. (*G*) Relative MitoTracker Red staining intensity within mitochondria was quantified using TOM20 to generate a mask of the mitochondrial area. HBECs were transfected with miR-23b-3p, miR-145-5p, or miR-494-3p mimics or NC for 72 hours from three independent experiments. Data shown represent the mean ± SEM in each group. *$P < 0.05$ and ***$P < 0.0005$. (*H*) Representative images of Hoechst 33342 and MitoSOX Red fluorescence staining in HBECs transfected with miR-23b-3p, miR-145-5p, or miR-494-3p inhibitors or NC. Treatment with IPF LF–derived EVs (10 μg/ml) was started 24 hours after transfection, and staining was performed after 48 hours of treatment. Scale bars, 100 μm. (*I*) Western blot using anti-p21, anti-p16, and anti–β-actin antibodies in HBECs transfected with miR-23b-3p inhibitor, miR-145–5p inhibitor, miR-494-3p inhibitor, or NC. Treatment with IPF LF–derived EVs (10 μg/ml) was started 24 hours after transfection, and protein samples were collected after 72 hours of treatment. The right panels show the average (±SEM) of relative expressions, which are taken from densitometric analysis of Western blot from three independent experiments. *$P < 0.05$, **$P < 0.005$, and ***$P < 0.0005$. (*J*) Gene-set enrichment analysis (GSEA) of HBECs transfected with miR-23b-3p and miR-494–3p mimics, showing downregulation of oxidative phosphorylation. The *P* value was calculated by using GSEA. GO = Gene Ontology.

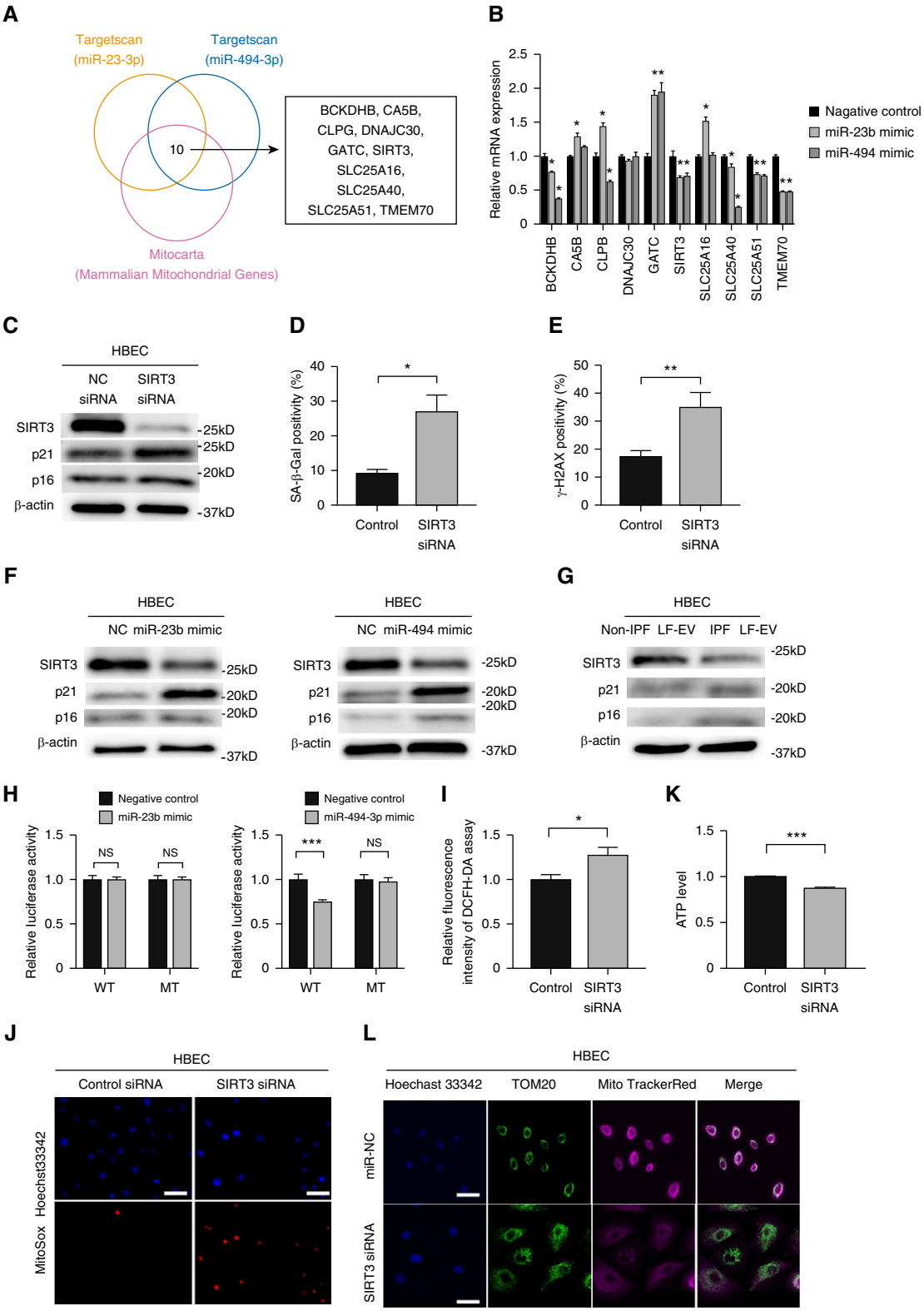

Figure 5. Reduced expression of SIRT3 (Sirtuin 3) is involved in miR-23b-3p– and miR-494-3p–mediated mitochondrial damage and cellular senescence. (*A*) A Venn diagram of the candidate target miRNAs of miR-23b-3p and miR-494-3p illustrating *in silico* analysis. (*B*) Quantitative real-time PCR analysis of the 10 candidate target mRNAs of miR-23b-3p and miR-494-3p in HBECs transfected with miR-23b-3p mimic, miR-494-3p mimic, or NC. *$P < 0.05$. (*C*) Western blot using anti-SIRT3, anti-p21, anti-p16, and anti–β-actin antibodies in HBECs transfected with SIRT3 siRNA or NC siRNA for 72 hours. (*D*) The percentage (±SEM) of SA-β-gal–positive HBECs transfected with SIRT3 siRNA or NC siRNA from three independent experiments for 72 hours. *$P < 0.05$.

25 Member 51), and *TMEM70* (Transmembrane Protein 70) were significantly decreased in HBECs after transfection with either miR-23b-3p or miR-494-3p mimics (Figure 5B). To determine which of these five candidate miRNA targets might be involved in regulating cellular senescence, we transfected HBECs with siRNAs targeting *SIRT3*, *BCKDHB*, *SLC25A40*, *SLC25A51*, or *TMEM70*. Knockdown of *SIRT3* clearly increased p21 and p16 expression, SA-β-gal positivity, and the number of γ-H2AX foci in HBECs (Figures 5C–5E, E5A, and E5B). In contrast, *BCKDHB*, *SLC25A40*, *SLC25A51*, and *TMEM70* knockdown had no effect on p16 and p21 expression in HBECs (Figures E5C–E5F). We confirmed that SIRT3 protein levels were decreased in HBECs after transfection with miR-23b-3p and miR-494-3p (Figure 5F). Importantly, SIRT3 expression was also decreased in HBECs that were treated with IPF LF–derived EVs (Figure 5G). These results strongly suggest that suppression of *SIRT3* expression by miR-23b-3p and miR-494-3p is responsible for promoting cellular senescence in HBECs treated with IPF LF–derived EVs. According to the *in silico* analysis, the 3′UTR region of *SIRT3* contains binding sites for both miR-23b-3p and miR-494-3p (Figure E5G). To confirm that miR-23b-3p and miR-494-3p actually bind to these regions, dual-luciferase reporter assays were performed. Although no significant changes in reporter activity were seen after transfection with miR-23b-3p, transfection with miR-494-3p significantly inhibited the activity of a firefly luciferase reporter controlled by the wild-type 3′UTR of *SIRT3*. This inhibition was lost after mutation of the SIRT3 3′UTR within the predicted miRNA binding site (Figure 5H), indicating that miR-494-3p may promote cellular senescence by directly targeting *SIRT3* in HBECs.

The causal link from reduced SIRT3 expression to mitochondrial damage and enhanced mtROS production was further established after SIRT3 knockdown in HBECs. Knockdown of *SIRT3* increased intracellular and mtROS levels (Figures 5I and 5J) and decreased both ATP levels and mitochondrial-membrane potential (Figures 5K and 5L) in HBECs. These results argue that miR-23b-3p– and miR-494-3p–mediated reduction of SIRT3 expression is at least partly responsible for the mitochondrial damage and senescence in HBECs that is induced by IPF LF–derived EVs.

Decreased SIRT3 Expression and Increased miR-23b-3p and miR-494–3p Expression in Lung Epithelial Cells Covering Fibrotic Lesions in IPF Lungs

Microarray analysis revealed significantly lower levels of SIRT3 expression in lung samples from patients with IPF than in healthy lungs (Figure 6A) (31). To further clarify the mechanism of SIRT3 involvement in accelerated epithelial-cell senescence in the lungs of patients with IPF, we analyzed the expression and distribution of SIRT3, miR-23b-3p and miR-494-3p in non-IPF and IPF lungs. Although SIRT3 expression was clearly detected in alveolar epithelial cells in non-IPF lungs and in nonfibrotic areas of IPF lungs, SIRT3 was barely detectable by immunocytochemistry in fibroblastic foci and in metaplastic epithelial cells covering fibrotic lesions in IPF lungs (Figure 6B). Bronchiolization and alveolar type II epithelial cells have pivotal roles in the initiation and progression of IPF pathogenesis (32), so SIRT3 expression in lung epithelial cells in both non-IPF and IPF lungs was also examined for colocalization with the ABCA3 (ATP binding cassette subfamily A member 3), which is a type II epithelial-cell marker (Figure 6C). In line with previous findings (33), reduced SIRT3 expression levels in type II epithelial cells from fibrotic lesions were assessed by quantitative evaluation of microscopic images of IPF lungs (Figure 6D). To further investigate the involvement of specific miRNAs in IPF pathogenesis, we used formalin-fixed paraffin-embedded lungs from patients without IPF ($n = 12$) and patients with IPF ($n = 8$) for laser-capture microdissection and quantitative real-time PCR analysis of miR-23b-3p and miR-494-3p expression levels in epithelial cells (Figure 6E). In comparison with non-IPF lungs, miR-23b-3p and miR-494-3p expression levels were significantly increased in epithelial cells from patients with IPF. Intriguingly, the expression levels of miR-23b-3p and miR-494-3p in LF-derived EVs from both patients without IPF and patients with IPF were significantly correlated with the percentage of vital capacity of the lungs from which the fibroblasts originated (Figure 6F), suggesting a pathogenic role for these miRNAs in the development of fibrosis in IPF.

Discussion

Our current studies identify a novel mode of EV cargo-mediated fibroblast–epithelial cell communication in lungs that results in epithelial-cell senescence (Figure 7). IPF fibroblasts secrete increased levels of EVs containing miR-23b-3p and miR-494-3p, which is shown to induce mitochondrial damage accompanied by enhanced mtROS production in lung epithelial cells, further leading to increased epithelial-cell DDR and senescence. The target of the miRNAs

Figure 5. (*Continued*). (*E*) The percentage of γ-H2AX–positive HBECs transfected with SIRT3 siRNA or control siRNA from three independent experiments for 48 hours. $^{**}P < 0.005$. (*F*) Western blot using anti-SIRT3, anti-p21, anti-p16, and anti–β-actin antibodies in HBECs transfected with miR-23b-3p, miR-494-3p, or NC. (*G*) Western blot using anti-SIRT3 and anti–β-actin antibodies in HBECs incubated with IPF LF–derived and non-IPF LF–derived EVs (10 μg/ml). (*H*) The effect of cotransfection of miR-23b-3p and miR-494-3p with WT and MT psiCHECK2 vectors with each gene construct in hman embryonic kidney 293 cells was measured using luciferase reporter assays. $^{***}P < 0.0005$. (*I*) Fluorescence intensity of DCFH-DA staining for intracellular ROS production. Incubation with DCFH-DA was started at 48 hours after transfection of SIRT3 siRNA in HBECs. Data shown represent the mean ± SEM of $n = 6$ in each group. $^{*}P < 0.05$. (*J*) Representative images of Hoechst 33342 and MitoSOX Red fluorescence staining in HBECs transfected with SIRT3 siRNA or control siRNA from three independent experiments for 48 hours. Scale bars, 100 μm. (*K*) Intracellular ATP levels were determined after transfection with SIRT3 siRNA or control siRNA for 72 hours in HBECs. Data shown represent the mean ± SEM of $n = 6$ in each group. $^{***}P < 0.0005$. (*L*) Representative fluorescence microscopy images showing cellular distribution of the mitochondria-specific dye MitoTracker Red (magenta) and TOM20 (green). HBECs were transfected with SIRT3 siRNA or control siRNA for 72 hours. Scale bars, 25 μm. *BCKDHB* = branched chain keto acid dehydrogenase E1 subunit β; *CA5B* = carbonic anhydrase 5B; *CLPB* = ClpB homolog, mitochondrial AAA ATPase chaperonin; *DNAJC30* = member C30; *GATC* = glutamyl-TRNA amidotransferase subunit C; MT = mutant; *SLC25A16* = solute carrier family 25 member 16; *SLC25A40* = solute carrier family 25 member 40; *SLC25A51* = solute carrier family 25 member 51; *TMEM70* = transmembrane protein 70; WT = wild type.

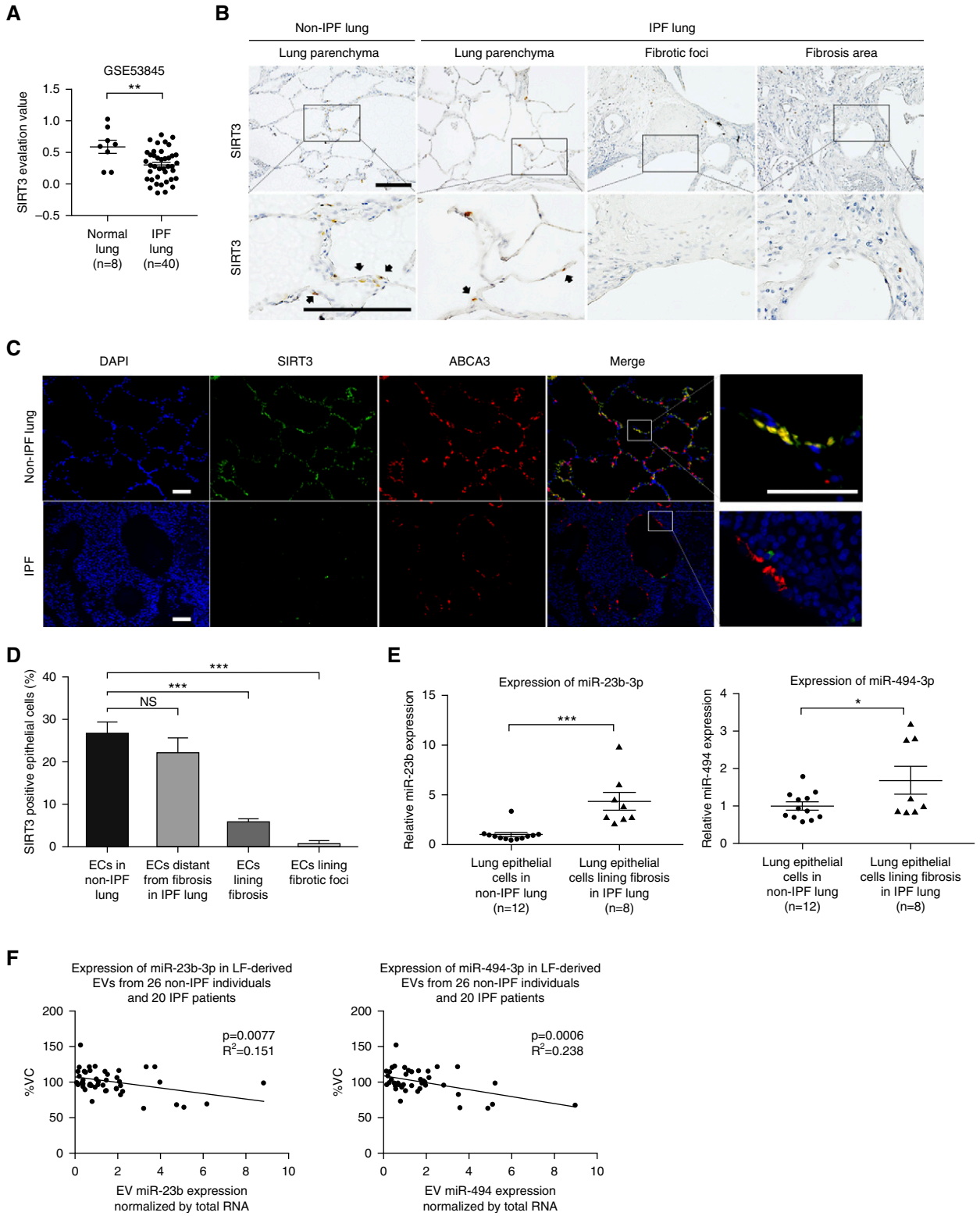

Figure 6. Decreased SIRT3 expression and increased miR-23b-3p and miR-494-3p expression in lung epithelial cells (ECs) covering fibrotic lesions in IPF lungs. (*A*) SIRT3 evaluation value in the mRNA microarray data set GSE53845 from the Gene Expression Omnibus database. $^{**}P < 0.005$. (*B*) Representative images of immunohistochemical analyses from IPF lungs using anti-SIRT3 antibody. Arrows indicate type II ECs. Scale bars, 100 μm. (*C*) Representative immunofluorescence using anti-SIRT3 antibody (green), anti-ABCA3 (ATP binding cassette subfamily A member 3) antibody (type II EC marker; red), and DAPI to stain nuclei (blue), illustrating low SIRT3 expression in lung ECs in IPF lungs. Scale bars, 50 μm. (*D*) Average of SIRT3-positive

appears to be SIRT3, as indicated by decreased expression of this protein. We used methods independent of EV-mediated transfer to confirm that miRNA-dependent loss of SIRT3 expression underlies the observed deleterious changes in lung epithelial cells.

Lung epithelial-cell senescence is crucial for the initiation and progression of fibrosis in IPF (3, 10). Although several factors, such as environmental-toxin exposure, depletion of antioxidant defenses, and telomere shortening, have been reported to be involved in the induction of epithelial cellular senescence, the specific mechanisms of epithelial-cell senescence in IPF remain largely unexplored (10, 34). In addition, elimination of senescent epithelial cells in a mouse model of lung fibrosis has been shown to attenuate the expression of both SASP factors and fibrotic markers (5). Accordingly, elucidation of the mechanisms that accelerate epithelial-cell senescence is critical not only for understanding IPF pathogenesis but also for developing novel treatment modalities for IPF. In this respect, our results are important for their identification of IPF LF–derived EVs as key mechanistic players in promoting senescence. Furthermore, the involvement of EVs in cellular senescence remains largely unknown (35). In particular, the senescent phenotype and the regulatory mechanisms induced by EVs have not yet been reported. Therefore, we identified a novel role for EV in accelerating cellular senescence by regulating ROS production of mitochondrial damage in recipient cells.

miRNAs can act as paracrine mediators of signaling in cases in which they are transferred between cells. EVs provide one means of accomplishing this type of intercellular transfer. Several studies have shown that EV-associated miRNAs are important modulators of lung homeostasis and some pulmonary diseases (19). However, the specific pathological roles of EVs in IPF lungs have not been fully studied (36–39). In this study, we demonstrate that miR-23b-3p and miR-494-3p released from fibroblasts as EV cargo are transferred to lung epithelial cells, where they induce mitochondrial damage and cellular senescence in HBECs. In previous studies, miR-23b-3p and miR-494-3p were shown to be involved in regulating a wide variety of cellular processes, including cell differentiation, proliferation, apoptosis, and cell-cycle progression. For instance, depending on the cell type, miR-23b-3p can play either antioxidant or prooxidant roles in ROS regulation (40). Another report demonstrates that miR-23b-3p regulates high glucose–induced cellular metabolic memory in diabetic retinopathy through the action of SIRT1, which is a well-known senescence regulator (41). In addition, miRNA-494-3p induces cellular senescence in lung-cancer cells (42) and regulates mitochondrial biogenesis (43). In a similar vein, our results demonstrate a clear causal link between miRNAs and cellular senescence via regulation of mitochondrial integrity during IPF pathogenesis.

Mitochondria have an essential role in the process of cellular senescence (44). Although multiple mitochondrial signaling pathways are known to induce cellular senescence (45), the role of mitochondria in cellular senescence can generally be associated with random molecular damage mediated by ROS (27, 28, 46). Recently, the accumulation of dysmorphic and dysfunctional mitochondria has been observed in alveolar type II epithelial cells in IPF lungs (29). Hence, we hypothesized that epithelial-cell senescence induced by IPF LF–derived EVs can result from increased mitochondrial damage. Supporting this notion, we found that IPF LF–derived EVs induce mitochondrial damage in HBECs, as evidenced by decreases in ATP production and reduced mitochondrial-membrane potential that was accompanied by enhanced ROS production. In addition, EV treatment also initiated the DDR, which is consistent with recent findings that mitochondrial damage induces persistent DDR and cellular senescence (27, 28). The ability of an antioxidant to regulate mtROS to efficiently inhibit cellular senescence induced by IPF LF–derived EVs in HBECs further suggests the involvement of mtROS in this process. Although the direct association between mtROS production and cellular senescence is still being debated (45, 47), our experimental results suggest that lung epithelial-cell senescence induced by IPF LF–derived EVs can be at least partly be attributed to mitochondrial damage associated with enhanced mtROS in HBECs.

SIRT3, a member of the sirtuin family of NAD-dependent deacetylases, is specifically localized in the mitochondrial inner membrane and matrix. SIRT3 activity can reduce ROS in many cell types by directly modulating antioxidant enzymes such as MnSOD and isocitrate dehydrogenase 2 (48). Recently, Jablonski and colleagues reported that a decrease in SIRT3 function in alveolar epithelial cells is one aspect of IPF pathogenesis (33). SIRT3 loss was associated with increased mtDNA damage and apoptosis in epithelial cells. Our results are consistent with this report, as they show that expression levels of SIRT3 are decreased in lung epithelial cells after treatment with IPF LF–derived EVs. In addition, SIRT3 has an essential role not only in apoptosis but also in cellular senescence (49), as determined by assessing the degree of DNA damage (50). In line with these findings, our knockdown of SIRT3 induced mitochondrial damage and cellular senescence in HBECs. Accordingly, it is likely that *SIRT3* suppression by miRNAs associated with IPF LF–derived EVs has an essential role in epithelial-cell senescence triggered by increased mitochondrial damage and the DDR (50).

There are several limitations to our study. First, the mechanisms suggested by our *in vitro* experiments have not been confirmed using *in vivo* models of pulmonary fibrosis. Although miR-494-3p in IPF LF–derived EVs suppresses *SIRT3* expression by binding directly to the 3′UTR of SIRT3 mRNA in primary human epithelial cells, the sequence of the 3′UTR region of SIRT3 is quite different between human and mouse cells. As a result, the mouse ortholog of miR-494-3p does not bind to the 3′UTR of *SIRT3* mRNA, rendering the use of mouse models somewhat problematic. Second, the direct target of miR-23b-3p in HBECs is not identified in this study. Relative-luciferase-activity assays have demonstrated that miR-23b-3p does not

Figure 6. (*Continued*). cells in lung ECs by quantification of microscopic images from four individuals without IPF and four patients with IPF. ***$P < 0.0005$. (*E*) Quantitative real-time PCR analysis of lung EC miRNA expressions obtained by laser capture from 12 individuals without IPF and 8 patients with IPF. RNU6B was used as an internal control. *$P < 0.05$ and ***$P < 0.0005$. (*F*) The relationship between relative validated EV-associated miRNA expressions from 26 individuals without IPF and 20 patients with IPF normalized to total RNA levels and the percentages of VC. VC = vital capacity.

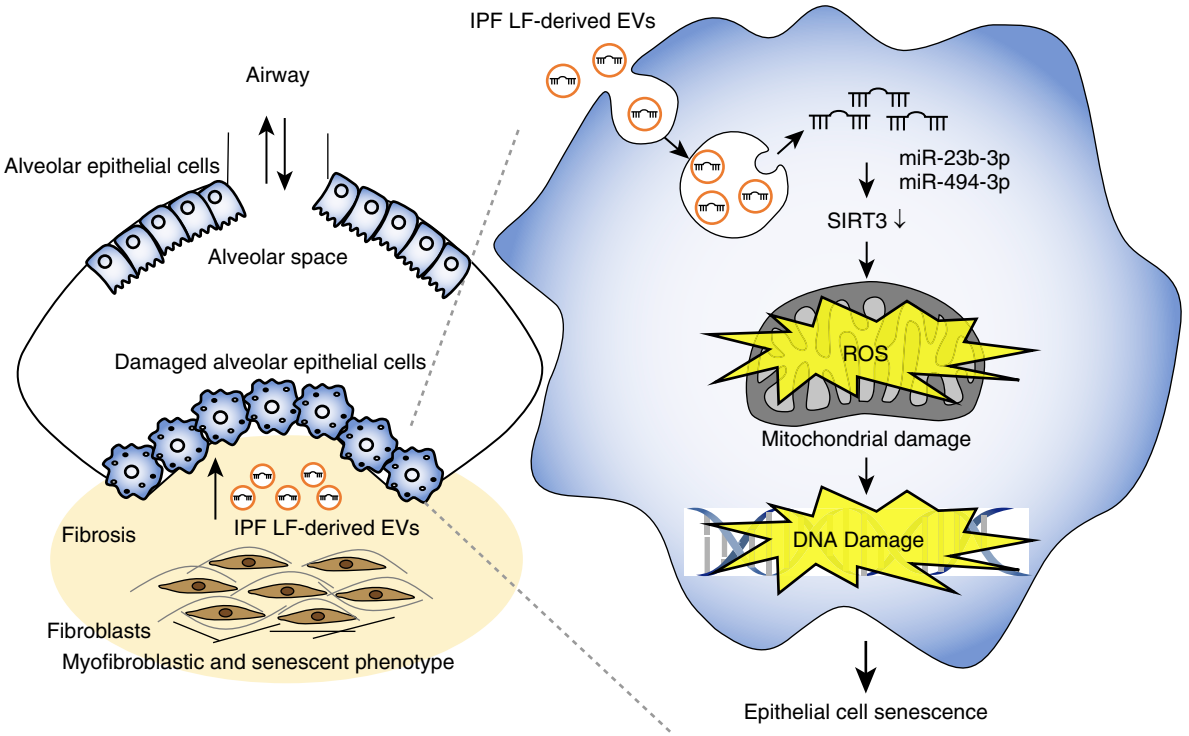

Figure 7. Schematic model of LF-derived EV-mediated EC senescence in IPF pathogenesis. LFs from patients with IPF induce EC senescence via the EV miRNA transfer to lung ECs. IPF LF–derived EVs increase mtROS and associated mitochondrial damage in lung ECs, leading to mtROS-mediated activation of the DNA damage response and subsequent EC senescence. Mechanistically, significantly upregulated miR-23b-3p and miR-494-3p in IPF LF–derived EVs are responsible for suppressing *SIRT3*, resulting in the EV-induced phenotypes in lung ECs.

inhibit the luciferase activity of the wild type of SIRT3, although transfection with a miR-23b-3p mimic suppresses the expression of SIRT3. This result suggests that miR-23b-3p either binds to another SIRT3 site, such as the 5′UTR or the coding-sequence regions, or regulates a gene upstream of SIRT3.

In summary, we have identified a novel epithelial–mesenchymal interaction that is mediated by LF-derived EVs. This interaction induces mitochondrial damage and senescence in epithelial cells during IPF pathogenesis. Accordingly, strategies for inhibiting specific miRNA species or blocking secretion of cell type–specific EVs may be developed as new geroprotective therapeutic options. ■

Author disclosures are available with the text of this article at www.atsjournals.org.

Acknowledgment: The authors thank Dr. Masahiro Yoshida, Dr. Kazuya Tsubouchi, Dr. Kenji Kobayashi, Dr. Yusuke Kurita, Dr. Nahoko Sato, Dr. Nayuta Saito, Dr. Akihiro Ichikawa, Dr. Yusuke Hosaka, and Dr. Akihiko Ito (Jikei University School of Medicine, Tokyo, Japan) for technical support and clinical-sample collection; Misato Yamamoto for excellent technical assistance; Dr. Nobuyoshi Kosaka for technical advice and helpful discussions; Dr. Katsutoshi Nakayama (Akita University) for data interpretation; Dr. Kurataka Otsuka and Dr. Yusuke Yamamoto (National Cancer Center Research Institute) for carefully reading the manuscript; and Dr. Odaka and Dr. Morikawa (Jikei University School of Medicine, Tokyo, Japan) for providing surgical samples.

References

1. Natsuizaka M, Chiba H, Kuronuma K, Otsuka M, Kudo K, Mori M, *et al*. Epidemiologic survey of Japanese patients with idiopathic pulmonary fibrosis and investigation of ethnic differences. *Am J Respir Crit Care Med* 2014;190:773–779.
2. Campisi J, d'Adda di Fagagna F. Cellular senescence: when bad things happen to good cells. *Nat Rev Mol Cell Biol* 2007;8:729–740.
3. Minagawa S, Araya J, Numata T, Nojiri S, Hara H, Yumino Y, *et al*. Accelerated epithelial cell senescence in IPF and the inhibitory role of SIRT6 in TGF-β-induced senescence of human bronchial epithelial cells. *Am J Physiol Lung Cell Mol Physiol* 2011;300:L391–L401.
4. Schafer MJ, White TA, Iijima K, Haak AJ, Ligresti G, Atkinson EJ, *et al*. Cellular senescence mediates fibrotic pulmonary disease. *Nat Commun* 2017;8:14532.
5. Lehmann M, Korfei M, Mutze K, Klee S, Skronska-Wasek W, Alsafadi HN, *et al*. Senolytic drugs target alveolar epithelial cell function and attenuate experimental lung fibrosis ex vivo. *Eur Respir J* 2017;50:1602367.
6. Naikawadi RP, Disayabutr S, Mallavia B, Donne ML, Green G, La JL, *et al*. Telomere dysfunction in alveolar epithelial cells causes lung remodeling and fibrosis. *JCI Insight* 2016;1:e86704.
7. King TE Jr, Pardo A, Selman M. Idiopathic pulmonary fibrosis. *Lancet* 2011;378:1949–1961.
8. Selman M, Pardo A. Role of epithelial cells in idiopathic pulmonary fibrosis: from innocent targets to serial killers. *Proc Am Thorac Soc* 2006;3:364–372.
9. Araya J, Kojima J, Takasaka N, Ito S, Fujii S, Hara H, *et al*. Insufficient autophagy in idiopathic pulmonary fibrosis. *Am J Physiol Lung Cell Mol Physiol* 2013;304:L56–L69.

10. Selman M, Pardo A. Revealing the pathogenic and aging-related mechanisms of the enigmatic idiopathic pulmonary fibrosis. an integral model. *Am J Respir Crit Care Med* 2014;189:1161–1172.
11. Huang SK, Scruggs AM, McEachin RC, White ES, Peters-Golden M. Lung fibroblasts from patients with idiopathic pulmonary fibrosis exhibit genome-wide differences in DNA methylation compared to fibroblasts from nonfibrotic lung. *PLoS One* 2014;9:e107055.
12. Lindahl GE, Stock CJ, Shi-Wen X, Leoni P, Sestini P, Howat SL, *et al*. Microarray profiling reveals suppressed interferon stimulated gene program in fibroblasts from scleroderma-associated interstitial lung disease. *Respir Res* 2013;14:80.
13. Ramos C, Montaño M, García-Alvarez J, Ruiz V, Uhal BD, Selman M, *et al*. Fibroblasts from idiopathic pulmonary fibrosis and normal lungs differ in growth rate, apoptosis, and tissue inhibitor of metalloproteinases expression. *Am J Respir Cell Mol Biol* 2001;24:591–598.
14. Uhal BD, Joshi I, True AL, Mundle S, Raza A, Pardo A, *et al*. Fibroblasts isolated after fibrotic lung injury induce apoptosis of alveolar epithelial cells *in vitro*. *Am J Physiol* 1995;269:L819–L828.
15. Waghray M, Cui Z, Horowitz JC, Subramanian IM, Martinez FJ, Toews GB, *et al*. Hydrogen peroxide is a diffusible paracrine signal for the induction of epithelial cell death by activated myofibroblasts. *FASEB J* 2005;19:854–856.
16. Kendall RT, Feghali-Bostwick CA. Fibroblasts in fibrosis: novel roles and mediators. *Front Pharmacol* 2014;5:123.
17. Kosaka N, Iguchi H, Yoshioka Y, Takeshita F, Matsuki Y, Ochiya T. Secretory mechanisms and intercellular transfer of microRNAs in living cells. *J Biol Chem* 2010;285:17442–17452.
18. Kosaka N, Iguchi H, Hagiwara K, Yoshioka Y, Takeshita F, Ochiya T. Neutral sphingomyelinase 2 (nSMase2)-dependent exosomal transfer of angiogenic microRNAs regulate cancer cell metastasis. *J Biol Chem* 2013;288:10849–10859.
19. Fujita Y, Kosaka N, Araya J, Kuwano K, Ochiya T. Extracellular vesicles in lung microenvironment and pathogenesis. *Trends Mol Med* 2015; 21:533–542.
20. Luga V, Zhang L, Viloria-Petit AM, Ogunjimi AA, Inanlou MR, Chiu E, *et al*. Exosomes mediate stromal mobilization of autocrine Wnt-PCP signaling in breast cancer cell migration. *Cell* 2012;151:1542–1556.
21. Boelens MC, Wu TJ, Nabet BY, Xu B, Qiu Y, Yoon T, *et al*. Exosome transfer from stromal to breast cancer cells regulates therapy resistance pathways. *Cell* 2014;159:499–513.
22. Araya J, Cambier S, Markovics JA, Wolters P, Jablons D, Hill A, *et al*. Squamous metaplasia amplifies pathologic epithelial-mesenchymal interactions in COPD patients. *J Clin Invest* 2007;117:3551–3562.
23. Richards KE, Zeleniak AE, Fishel ML, Wu J, Littlepage LE, Hill R. Cancer-associated fibroblast exosomes regulate survival and proliferation of pancreatic cancer cells. *Oncogene* 2017;36:1770–1778.
24. Chilosi M, Poletti V, Murer B, Lestani M, Cancellieri A, Montagna L, *et al*. Abnormal re-epithelialization and lung remodeling in idiopathic pulmonary fibrosis: the role of deltaN-p63. *Lab Invest* 2002;82:1335–1345.
25. d'Adda di Fagagna F. Living on a break: cellular senescence as a DNA-damage response. *Nat Rev Cancer* 2008;8:512–522.
26. Rodier F, Coppé J-P, Patil CK, Hoeijmakers WAM, Muñoz DP, Raza SR, *et al*. Persistent DNA damage signalling triggers senescence-associated inflammatory cytokine secretion. *Nat Cell Biol* 2009;11: 973–979. [Published erratum appears in Nat Cell Biol 11:1272.]
27. Moiseeva O, Bourdeau V, Roux A, Deschênes-Simard X, Ferbeyre G. Mitochondrial dysfunction contributes to oncogene-induced senescence. *Mol Cell Biol* 2009;29:4495–4507.
28. Correia-Melo C, Marques FDM, Anderson R, Hewitt G, Hewitt R, Cole J, *et al*. Mitochondria are required for pro-ageing features of the senescent phenotype. *EMBO J* 2016;35:724–742.
29. Bueno M, Lai Y-C, Romero Y, Brands J, St Croix CM, Kamga C, *et al*. PINK1 deficiency impairs mitochondrial homeostasis and promotes lung fibrosis. *J Clin Invest* 2015;125:521–538.
30. Calvo SE, Clauser KR, Mootha VK. MitoCarta2.0: an updated inventory of mammalian mitochondrial proteins. *Nucleic Acids Res* 2016;44: D1251–D1257.
31. DePianto DJ, Chandriani S, Abbas AR, Jia G, N'Diaye EN, Caplazi P, *et al*. Heterogeneous gene expression signatures correspond to distinct lung pathologies and biomarkers of disease severity in idiopathic pulmonary fibrosis. *Thorax* 2015;70:48–56.
32. Sisson TH, Mendez M, Choi K, Subbotina N, Courey A, Cunningham A, *et al*. Targeted injury of type II alveolar epithelial cells induces pulmonary fibrosis. *Am J Respir Crit Care Med* 2010;181:254–263.
33. Jablonski RP, Kim S-J, Cheresh P, Williams DB, Morales-Nebreda L, Cheng Y, *et al*. SIRT3 deficiency promotes lung fibrosis by augmenting alveolar epithelial cell mitochondrial DNA damage and apoptosis. *FASEB J* 2017;31:2520–2532.
34. Alder JK, Chen JJ-L, Lancaster L, Danoff S, Su S-C, Cogan JD, *et al*. Short telomeres are a risk factor for idiopathic pulmonary fibrosis. *Proc Natl Acad Sci USA* 2008;105:13051–13056.
35. Kadota T, Fujita Y, Yoshioka Y, Araya J, Kuwano K, Ochiya T. Emerging role of extracellular vesicles as a senescence-associated secretory phenotype: insights into the pathophysiology of lung diseases. *Mol Aspects Med* 2018;60:92–103.
36. Martin-Medina A, Lehmann M, Burgy O, Hermann S, Baarsma HA, Wagner DE, *et al*. Increased extracellular vesicles mediate WNT5A signaling in idiopathic pulmonary fibrosis. *Am J Respir Crit Care Med* 2018;198:1527–1538.
37. Chanda D, Otoupalova E, Hough KP, Locy ML, Bernard K, Deshane JS, *et al*. Fibronectin on the surface of extracellular vesicles mediates fibroblast invasion. *Am J Respir Cell Mol Biol* 2019;60:279–288.
38. Makiguchi T, Yamada M, Yoshioka Y, Sugiura H, Koarai A, Chiba S, *et al*. Serum extracellular vesicular miR-21-5p is a predictor of the prognosis in idiopathic pulmonary fibrosis. *Respir Res* 2016;17:110.
39. Njock M-S, Guiot J, Henket MA, Nivelles O, Thiry M, Dequiedt F, *et al*. Sputum exosomes: promising biomarkers for idiopathic pulmonary fibrosis. *Thorax* 2019;74:309–312.
40. Donadelli M, Dando I, Fiorini C, Palmieri M. Regulation of miR-23b expression and its dual role on ROS production and tumour development. *Cancer Lett* 2014;349:107–113.
41. Zhao S, Li T, Li J, Lu Q, Han C, Wang N, *et al*. miR-23b-3p induces the cellular metabolic memory of high glucose in diabetic retinopathy through a SIRT1-dependent signalling pathway. *Diabetologia* 2016; 59:644–654.
42. Ohdaira H, Sekiguchi M, Miyata K, Yoshida K. MicroRNA-494 suppresses cell proliferation and induces senescence in A549 lung cancer cells. *Cell Prolif* 2012;45:32–38.
43. Yamamoto H, Morino K, Nishio Y, Ugi S, Yoshizaki T, Kashiwagi A, *et al*. MicroRNA-494 regulates mitochondrial biogenesis in skeletal muscle through mitochondrial transcription factor A and Forkhead box j3. *Am J Physiol Endocrinol Metab* 2012;303: E1419–E1427.
44. López-Otín C, Blasco MA, Partridge L, Serrano M, Kroemer G. The hallmarks of aging. *Cell* 2013;153:1194–1217.
45. Ziegler DV, Wiley CD, Velarde MC. Mitochondrial effectors of cellular senescence: beyond the free radical theory of aging. *Aging Cell* 2015;14:1–7.
46. Passos JF, Nelson G, Wang C, Richter T, Simillion C, Proctor CJ, *et al*. Feedback between p21 and reactive oxygen production is necessary for cell senescence. *Mol Syst Biol* 2010;6:347.
47. Leadsham JE, Sanders G, Giannaki S, Bastow EL, Hutton R, Naeimi WR, *et al*. Loss of cytochrome c oxidase promotes RAS-dependent ROS production from the ER resident NADPH oxidase, Yno1p, in yeast. *Cell Metab* 2013;18:279–286.
48. Someya S, Yu W, Hallows WC, Xu J, Vann JM, Leeuwenburgh C, *et al*. Sirt3 mediates reduction of oxidative damage and prevention of age-related hearing loss under caloric restriction. *Cell* 2010;143:802–812.
49. Wiley CD, Velarde MC, Lecot P, Liu S, Sarnoski EA, Freund A, *et al*. Mitochondrial dysfunction induces senescence with a distinct secretory phenotype. *Cell Metab* 2016;23:303–314.
50. Childs BG, Baker DJ, Kirkland JL, Campisi J, van Deursen JM. Senescence and apoptosis: dueling or complementary cell fates? *EMBO Rep* 2014;15:1139–1153.